Synthesis, structure and properties of an organic–inorganic hybrid independent 1-D double-chain Keggin-type silicotungstate with mixed ligands

Jie Luo, Xing Ma, Lijuan Chen *, Junwei Zhao *

Henan Key Laboratory of Polyoxometalate Chemistry, Institute of Molecule and Crystal Engineering, College of Chemistry and Chemical Engineering, Henan University, Kaifeng, Henan 475004, PR China

ABSTRACT

A novel organic–inorganic hybrid independent 1-D double-chain silicotungstate $[Cu(biim)_2][Cu(4,4'-bpy)(biim)(H_2O)][\alpha-SiW_{12}O_{40}]\cdot 3H_2O$ (**1**, biim = 2,2′-biimidazole, 4,4′-bpy = 4,4′-dipyridine) has been successfully synthesized by reaction of $Na_{10}[A-\alpha-SiW_9O_{34}]\cdot 18H_2O$, $CuCl_2\cdot 2H_2O$, $EuCl_3$, biim and 4,4′-bpy under 160 °C hydrothermal environment and characterized by elemental analyses, IR spectra and single-crystal X-ray diffraction. The most remarkable structural feature of **1** is that two types of independent 1-D chains are paralleling and one is constructed from plenary Keggin $[\alpha-SiW_{12}O_{40}]^{4-}$ units and $[Cu(biim)_2]^{2+}$ linkers while the other is based on $[Cu(biim)(H_2O)]^{2+}$ cations and 4,4′-bpy connectors. The variable-temperature magnetic susceptibility of **1** shows the weak antiferromagnetic exchange interactions within Cu^{II} centers. Furthermore, the solid-state electrochemical properties of **1** have been also measured in 0.5 mol·L^{-1} Na_2SO_4 + H_2SO_4 aqueous solution by entrapping it in a carbon paste electrode.

© 2015 Elsevier B.V. All rights reserved.

Polyoxometalates (POMs) are a large family of polynuclear mental–oxo clusters that are composed of the early transition-metals (TMs) in their highest oxidation states, like Mo^{VI}, W^{VI}, V^V, Nb^V and Ta^V [1]. Since the first POM $(NH_4)_3PMo_{12}O_{40}$ was reported 188 years ago [2], POM chemistry has attracted continuous research interest because of the remarkable and diverse structures and fascinating physical and chemical properties such as catalysis, sorption, separation, magnetic properties, acidities, and redox properties [3]. Among POMs, the design and synthesis of novel TM containing silicotungstates (STs) have become a research hotspot not only because the nucleophilic oxygen-enriched surface of STs can make them work as useful inorganic multidentate building blocks to capture TM cations, but also because TMs containing STs are ideal models for researching magnetic exchange interactions within TM centers [4,5]. Some typical findings are $[Mn_{19}(OH)_{12}(SiW_{10}O_{37})_6]^{34-}$ [6], $[\{M(OH_2)_2(\mu_3-OH)\}_2\{Zn(OH_2)\}_2\{\gamma-HSiW_{10}O_{36}\}_2]^{8-}$ (M = Co^{II}, Ni^{II}) [7], $[Ni_6(\mu_3-OH)_3(H_2O)_9SiW_9O_{34}]_2^{2-}$ [8], $[\{Na_3(\mu-OH_2)_2Co_2(\mu-OH)_4\}(Si_2W_{18}O_{66})]^{13-}$ and $[Na(H_2O)\{Co(H_2O)_3\}_2\{Co(H_2O)_2\}(Si_2 W_{18}O_{66})]^{9-}$ [9]. Moreover, lanthanides (Lns) containing STs have also been exploited due to the oxophilicity and high coordination number of Ln cations and their interesting magnetism, luminescence as well as Lewis acid catalysis [5]. To date, some Lns containing STs have been synthesized such as $[Ln_2(H_2O)_7 Si_2W_{18}O_{66}]^{10-}$ (Ln = Gd^{III}, Tb^{III}, Ho^{III}) [10],

$\{[Lu(pydc)(H_2O)_3]_3 [SiW_{12}O_{40}]\}^-$ [11] and $[\{RE(H_2O)_2(acetone)\}_2\{\gamma-SiW_{10}O_{36}\}_2]^{10-}$ (RE = Y^{III}, Nd^{III}, Eu^{III}, Gd^{III}, Tb^{III}, Dy^{III}) [12]. Currently, the design and preparation of novel POM-based TM–Ln heterometallic derivative (PBTLHD) with interesting structural topologies and properties have attracted increasing attention. Since the first PBTLHD was discovered by Wang et al. in 2004, great effort has been engaged in this field [13]. Nevertheless, the competitive reaction among highly negative POM precursors, strongly oxyphilic Ln cations and less active TM cations in the same reaction system is inevitable, which brings great difficulties to the discovery of PBTLHD [5]. It's found that the copper cation may overcome this obstacle because it has flexible coordination geometries (trigonal bipyramid, square pyramid and octahedron) and owns the Jahn–Teller effect of the octahedra and pseudo Jahn–Teller effect of the square pyramids [14]. Moreover, the trivacant Keggin-type $[A-\alpha-SiW_9O_{34}]^{10-}$ precursor can transform and isomerize to $[B-\alpha-SiW_9O_{34}]^{10-}$, $[\alpha-SiW_{11}O_{39}]^{8-}$, $[\alpha-SiW_{12}O_{40}]^{4-}$ and $[\beta-SiW_8O_{31}]^{10-}$ intermediates during the course of the reaction, and offer greater possibilities to simultaneously capture copper and Ln cations. Furthermore, organic N-ligands can help to construct extended architectures [15]. Starting from the concept of rational design, we explored the reactions of the trivacant Keggin-type $[A-\alpha-SiW_9O_{34}]^{10-}$ precursor with copper, Ln cations and organic components under hydrothermal conditions. In 2012, a class of novel 1-D double-chain ST-based Cu–Ln heterometallic hybrids $[Cu(dap)_2 (H_2O)]_2\{Cu(dap)_2[\alpha-H_2SiW_{11}O_{39}Ln(H_2O)_3]_2\}\cdot xH_2O$ (Ln = Ce^{III}, Gd^{III}, Er^{III}, x = 9; Ln = Pr^{III}, Nd^{III}, Sm^{III}, Eu^{III}, x = 10; Ln = Tb^{III}, Dy^{III}, x = 8) was successfully synthesized by our group [16]. Three 3-D

* Corresponding authors.
E-mail addresses: ljchen@henu.edu.cn (L. Chen), zhaojunwei@henu.edu.cn (J. Zhao).

organic–inorganic hybrid heterometallic STs assembled from 1:2-type $[Ln(\alpha\text{-SiW}_{11}O_{39})_2]^{13-}$ units and $[Cu(dap)_2]^{2+}$ linkers NaH $[Cu(dap)_2(H_2O)][Cu(dap)_2]_{4.5}[Ln(\alpha\text{-SiW}_{11}O_{39})_2]\cdot 7H_2O$ (Ln = Sm^{III}, Dy^{III}, Gd^{III}) were obtained in the same year [17]. Subsequently, an organic–inorganic hybrid 1-D double-chain copper–yttrium heterometallic ST $\{[Cu(dap)_2(H_2O)]_2\{Cu(dap)_2[\alpha\text{-H}_2SiW_{11}O_{39}Y\ (H_2O)_2]_2\}\cdot 10H_2O$ was reported by us in 2013 [18]. As a continuation of our work, biim and 4,4′-bpy as organic ligands were used to initiate exploitation. Unexpectedly, we obtained a neoteric organic–inorganic hybrid independent 1-D double-chain ST $[Cu(biim)_2][Cu(4,4'\text{-bpy})(biim)(H_2O)][\alpha\text{-SiW}_{12}O_{40}]\cdot 3H_2O$ (**1**) (biim = 2,2′-biimidazole, 4,4′-bpy = 4,4′-dipyridine). Unfortunately, it was not a PBTLHD.

1 was prepared as follows: after a mixture of $Na_{10}[A\text{-}\alpha\text{-SiW}_9O_{34}]\cdot 18H_2O$ (0.150 g, 0.539 mmol), $CuCl_2\cdot 2H_2O$ (0.220 g, 1.290 mmol), $EuCl_3$ (0.050 g, 0.194 mmol), biim (0.05 g, 0.373 mmol), 4,4′-bpy (0.030 g, 0.192 mmol) and H_2O (6 mL, 333 mmol) was stirred for 2.5 h (pH$_i$ = 4.13), sealed in a 25 mL Teflon-lined steel autoclave, kept at 160 °C for 5 days and then cooled to room temperature (pH$_f$ = 4.75), black cubic crystals were obtained by filtering, washed with distilled water and dried in air at ambient temperature. Yield: ca. 33% (based on $Na_{10}[A\text{-}\alpha\text{-SiW}_9O_{34}]\cdot 18H_2O$). Anal. calcd. (found %) for $C_{28}H_{34}Cu_2N_{14}O_{44}SiW_{12}$ (**1**): C 9.26 (9.37), H 0.94 (1.07), N 5.40 (5.20), Si 0.77 (0.75), Cu 3.50 (3.68), and W 60.74 (60.62). It is noteworthy that $Na_{10}[A\text{-}\alpha\text{-SiW}_9O_{34}]\cdot 18H_2O$ was employed during the course of preparing **1**, nevertheless, the $[\alpha\text{-SiW}_{12}O_{40}]^{4-}$ segment is observed in **1**. This phenomenon indicates that the transformation of $[A\text{-}\alpha\text{-SiW}_9O_{34}]^{10-}$ polyoxoanion (POA) → $[\alpha\text{-SiW}_{12}O_{40}]^{4-}$ POA happened in the formation of **1**. Although the transformation of trivacant Keggin POAs to monovacant Keggin POAs were observed in our previous investigations [16–18], the transformation of trivacant Keggin POA to plenary Keggin POA was rarely reported. However, though $EuCl_3$ was used in the reaction, Eu^{3+} ion was not found in **1**. Subsequently, the reaction with the removal of $EuCl_3$ was explored under the similar conditions unexpectedly, **1** wasn't obtained, which indicates the synergistic effect of $EuCl_3$ with other components in the formation of **1**. Similar phenomena have been previously encountered [19].

Single-crystal X-ray diffraction analysis [20] indicates that **1** crystallizes in the monoclinic space group $P2_1/m$. The basic molecular structural unit $[Cu(biim)_2][Cu(4,4'\text{-bpy})(biim)(H_2O)]\ [\alpha\text{-SiW}_{12}O_{40}]\cdot 3H_2O$ of **1** is composed of a plenary Keggin-type $[\alpha\text{-SiW}_{12}O_{40}]^{4-}$ POA, a pendant $[Cu2(biim)(H_2O)]^{2+}$ cation, a bridging $[Cu1(biim)_2]^{2+}$ cation, a bridging 4,4′-bpy ligand and three lattice water molecules. **1** exhibits the novel 1-D organic–inorganic zigzag double-chain architecture (Fig. 1a). Due to the existence of the octahedral geometry of the Cu1 cation in **1**, the Jahn–Teller effect occurs and gives rise to the slightly elongation of the Cu–O distances. What's more, the Cu1 cation in the ligand field displays the distorted octahedral geometry which may overcome the large steric hindrance and then help to increase the stability of **1**. Therefore the weak Cu–O interaction will be considered in the following description [21]. In the asymmetrical structural unit, the plenary Keggin-type $[\alpha\text{-SiW}_{12}O_{40}]^{4-}$ POA consists of a centered SiO$_4$ group with four corner-shared W$_3$O$_{13}$ triads and in each W$_3$O$_{13}$ triad three WO$_6$ octahedra are fused together in the edge-sharing mode. The centered Si atom displays a tetrahedral coordination geometry defined by four μ_4-oxygen atoms from three W$_3$O$_{13}$ triads with the Si–O distances of 1.616(9)–1.651(9) Å, and all W centers exhibit the octahedral coordination environment with the W–O distances of 1.679(10)–2.373(9) Å (Fig. 1b). Bond valence sum (BVS) calculations illustrate that the oxidation states of Si, W and Cu atoms in **1** are +4, +6 and +2, respectively. The $[Cu1(biim)_2]^{2+}$ cations link to the $[\alpha\text{-SiW}_{12}O_{40}]^{4-}$ POAs via the terminal oxygen atoms to develop the organic–inorganic zigzag 1-D chain and are embedded in the slightly distorted $\{CuO_2N_4\}$ octahedral geometry, in which four nitrogen atoms from two biim ligands occupy the basal plane [Cu–N: 1.999(8)–2.001(8) Å] and two terminal oxygen atoms from two $[\alpha\text{-SiW}_{12}O_{40}]^{4-}$ POAs [Cu–O: 2.528(7) Å] stand on two axial positions.

The $[Cu1(biim)_2]^{2+}$ cation displays the slightly elongated octahedral geometry, from which it can be easily concluded that the Cu1 cation has the electron configuration of $(t_{2g})^6(d_{x2-y2})^1(d_{z2})^2$. Focus on the neighboring chain, it's evident that the $[Cu2(biim)(H_2O)]^{2+}$ cations are connected with each other by the 4,4′-bpy linkers to finish the zigzag chain architecture. The square pyramid geometry of $[Cu2(biim)(H_2O)]^{2+}$ cation is defined by one oxygen atom from a water ligand [Cu–O: 2.261(2) Å], four nitrogen atoms from two 4,4′-bpy ligands and one biim ligand [Cu–N: 2.009(9)–2.058(9) Å] (Fig. 1c). Two obvious discrepancies between Cu1 and Cu2 cations are observed: (1) the Cu2 cation exhibits a square pyramid coordination environment while the Cu1 adopts an octahedral geometry; (2) the bridging Cu1 cation links to two biim ligands and then grafts to the $[\alpha\text{-SiW}_{12}O_{40}]^{4-}$ POA through the terminal oxygen atom constructing one 1-D zigzag chain whereas the Cu2 cation is combined with one biiim ligand and two 4,4′-bpy ligands to form the other 1-D zigzag chain.

If you go back to the history of POM chemistry, several intriguing 1-D chains based on Keggin-type ST units were reported. For example, Pope and co-workers communicated two 1-D inorganic zigzag chain Ln-containing monovacant Keggin STs $[Ln\ (\alpha\text{-SiW}_{11}O_{39})(H_2O)_3]^{5-}$ (Ln = Ce^{III}, La^{III}) in 2000 [22]. In 2003, Mialane et al. discovered a 1-D inorganic linear $[Yb(\alpha\text{-SiW}_{11}O_{39})\ (H_2O)_2]^{5-}$ chain and a 1-D zigzag $[Nd_2(\alpha\text{-SiW}_{11}O_{39})(H_2O)_{11}]^{2-}$ chain [23]. In 2004, Niu's group reported a 1-D inorganic zigzag chain $K_3\{[Pr(H_2O)_4(\alpha\text{-SiW}_{11}O_{39})](NaPr_2(H_2O)_{12})[Pr(H_2O)_4(\alpha\text{-SiW}_{11}O_{39})]\}\cdot 13H_2O$ [24], later they communicated another organic–inorganic hybrid ST-based Sm^{III}-containing 1-D double-chain $[Sm_2(\alpha\text{-SiW}_{11}\ O_{39})(DMSO)_3(H_2O)_6]^{2-}$ in 2006 [25]. In 2010, an inorganic ST-based Cr^{III}–La^{III} heterometallic 1-D double-chain $Cs_4[(\gamma\text{-SiW}_{10}O_{36})_2\ (Cr(OH)(H_2O))_3(La(H_2O)_7)_2]\cdot 19H_2O$ was addressed by Compain et al. [26]. In succession, our group discovered a kind of novel 1-D double-chain ST-based Cu–Ln heterometallic hybrids (**2**) [16,18]. Compared with the 1-D double-chain previously reported by us, the innovation of **1** should be highlighted: (a) **1** represents the first organic–inorganic hybrid 1-D double-chain that is created by the plenary Keggin moieties, whereas **2** is formed by the mono-Ln substituted Keggin moieties; (b) the most remarkable structure characteristic is that two organic–inorganic chains in **1** are independent while **2** owns two same and antiparallel chains that link to each other by $[Cu_2(dap)_2]^{2+}$ cations.

In order to highlight the structure of **1**, we take the $[Cu1(biim)_2]^{2+}$ and 4,4′-bpy bridges as connectors with two colors and reckon the plenary $[\alpha\text{-SiW}_{12}O_{40}]^{4-}$ POAs as triangular pyramids and $[Cu2(biim)(H_2O)]^{2+}$ cations as nodes. This simplified graph with two kinds of 1-D zigzag chains along the a axis is shown in Fig. 1d. The zigzag angle of the $\{[Cu(biim)_2][\alpha\text{-SiW}_{12}O_{40}]\}_n^{2n-}$ chain is 68.097(1)° while the zigzag angle of the $[Cu(4,4'\text{-bpy})(biim) (H_2O)]_n^{n+}$ chain is 95.817(1)°. In the zigzag angle of the $\{[Cu(biim)_2][\alpha\text{-SiW}_{12}O_{40}]\}_n^{2n-}$ chain the distance of two conjoint triangular pyramids is 14.8873(41) Å whereas the distance of two conjoint Cu2 nodes is 11.2324(20) Å in the $[Cu(4,4'\text{-bpy})(biim) (H_2O)]_n^{n+}$ chain. In addition, the distance of two adjacent nodes (or POAs) in the same side of each zigzag chain is 16.6705(17) Å (Fig. S1). Interestingly, the adjacent plenary Keggin-type $[\alpha\text{-SiW}_{12}O_{40}]^{4-}$ POAs in the zigzag $\{[Cu(biim)_2][\alpha\text{-SiW}_{12}O_{40}]\}_n^{2n-}$ chain exhibits two types of spatial orientation (Fig. 1e). Viewed along the a axis (Fig. 1f), the $\{[Cu(biim)_2][\alpha\text{-SiW}_{12}O_{40}]\}_n^{2n-}$ chains and the $\{[Cu(biim)_2][\alpha\text{-SiW}_{12}O_{40}]\}_n^{2n-}$ chains are alternatively aligned. Fig. 1g illustrates the schematic packing in the ac plane, which displays that two types of 1-D zigzag chains are not perpendicular to each other.

The IR spectrum of **1** is collected from a solid sample palletized with KBr in the range of 4000–400 cm^{-1} and exhibits the characteristic vibration pattern derived from the plenary Keggin ST framework. Four characteristic vibration bands, namely, terminal $\nu_{as}(W\text{–}O_t)$, $\nu_{as}(Si\text{–}O_a)$, corner-sharing $\nu_{as}(W\text{–}O_b)$, edge-sharing $\nu_{as}(W\text{–}O_c)$, appear at 980, 920, 883, and 796 cm^{-1}, respectively (Fig. S2). As a rule, these
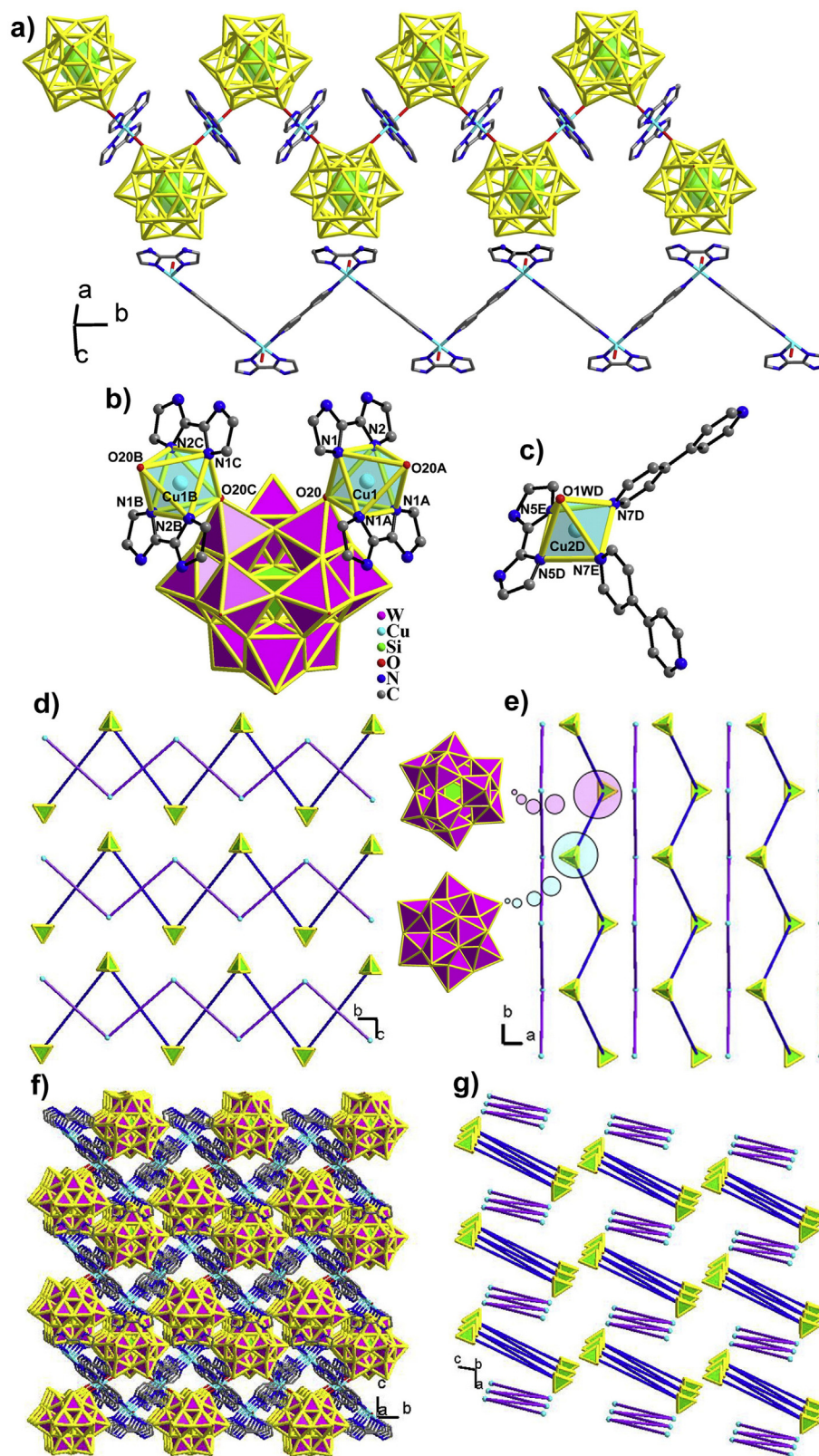
Fig. 1. (a) The view of two 1-D chains in **1**. (b) The view of a plenary $[\alpha\text{-}SiW_{12}O_{40}]^{4-}$ POA connecting to two bridging $[Cu1(biim)_2]^{2+}$ cations in **1** with the selected numbering scheme. The distorted octahedral geometry of the $[Cu1(biim)_2]^{2+}$ cation is highlighted. (c) The view of the square pyramidal coordination environment of the $[Cu2(biim)(H_2O)]^{2+}$ cation. Lattice water molecules and hydrogen atoms attached to carbon and nitrogen atoms are omitted for clarity. The atoms with "A, B, C, D, E" are generated by the symmetry operation. A: $2 - x$, $-y$, $-z$; B: $2 - x$, $0.5 + y$, $-z$, C: x, $0.5 - y$, z, D: $1 - x$, $-0.5 + y$, $2-z$, E: $1 - x$, $-y$, $2 - z$. (d) The simplified packing of two types of 1-D zigzag chains in **1** viewed along the a axis. ($[\alpha\text{-}SiW_{12}O_{40}]^{4-}$ POA: triangular pyramid, $[Cu2(biim)(H_2O)]^{2+}$ cations: light blue spheres, all ligands and water molecules are omitted for clarity). (e) The simplified packing of two types of 1-D zigzag chains in **1** viewed along the c axis. (f) The packing of two types of 1-D zigzag chains in **1** in the bc plane. (g) The simplified packing of two types of 1-D zigzag chains in **1** in the ac plane.

characteristic bands can be readily identified in comparison with the corresponding bands of plenary Keggin POT clusters [27]. It can be found that the ν_{as}(terminal W–O_t) vibration band in **1** is almost not shifted, suggesting the weak interactions between the [Cu1(biim)$_2$]$^{2+}$ cations and the terminal oxygen atoms of [α-SiW$_{12}$O$_{40}$]$^{4-}$ framework, which is in good agreement with the long Cu–O_t distance [Cu–O: 2.528(7) Å] in **1**. It is obvious that four characteristic vibration bands of **1** are different from the precursor Na$_{10}$[A-α-SiW$_9$O$_{34}$]·18H$_2$O [931, 862, 806 and 694 cm^{-1} for ν_{as}(W–O_t), ν_{as}(Si–O_a), ν_{as}(W–O_b) and ν_{as}(W–O_c)] (Fig. S3), which further indicates the evolution from [A-α-SiW$_9$O$_{34}$]$^{10-}$ to [α-SiW$_{12}$O$_{40}$]$^{4-}$ in the formation of **1**. Comparing to the IR spectra of 4,4′-bpy and biim (Fig. S4), two vibration peaks at 1415 and 1218 cm^{-1} denote the presence of 4,4′-bpy in **1** [28] and three vibration peaks at 3144, 2841 and 1529 cm^{-1} are indicative of the occurrence of biim in **1** [29]. Furthermore, the stretching vibration peak and bending vibration absorption peak of lattice water molecules or coordination water molecules are observed at the 3490 and 1610 cm^{-1}, respectively.

Since the electrochemistry of POMs was reported by Toth and Anson in 1989 [30], great efforts have been devoted to the study of the electrochemistry of POMs partly because POMs as electron reservoirs can deliver electrons to other species in the redox processes [31]. In this context, cyclic voltammetry (CV) experiment was performed to examine the solid-state electrochemical properties of **1** in 0.5 mol·L^{-1} Na$_2$SO$_4$ + H$_2$SO$_4$ aqueous solution by manufacturing **1**-CPE (carbon paste electrode). **1** shows the four groups of redox waves involving W^{VI} and Cu^{II} centers. It is obvious that in the pH = 4.15 sulfate medium, the typical CV behavior of **1** (Fig. 2a) at a scan rate of 20 mV s^{-1} at room temperature shows four couples of redox waves at $E_{1/2} = -0.803$ V (I/I′), $E_{1/2} = -0.565$ V (II/II′), $E_{1/2} = -0.173$ V (III/III′) and $E_{1/2} = 0.144$ V (IV/IV′) [$E_{1/2} = (E_{pa} + E_{pc}) / 2$]. The first three oxidation peaks I, II and III (-0.731 V, -0.479 V and -0.029 V, respectively) and their reduction counterparts I′, II′ and III′ (-0.875 V, -0.651 and -0.371 V) feature the redox processes of W centers in the ST polyoxoanion [32]. Moreover, their peak potential separations of the W based waves are around 144 mV, 172 mV and 288 mV, respectively, which may correspond to three irreversible one-electron charge-transfer processes. The last oxidation peak IV ($+0.262$ V) and its reduction counterpart IV′ ($+0.026$ V) are attributed to the redox process of the Cu^{II} centers and the peak potential separation of 236 mV indicates that the redox procedure of the Cu^{II} center is irreversible [33].

In order to probe the influence of the variation of the acidity on the electrochemical response of **1**-CPE, H$_2$SO$_4$ was used to adjust the pH values of medium. The results indicate that the electrochemical behavior of **1**-CPE is pH dependent. As the pH decreases from 4.44 to 2.66, the redox wave shifts to the negative potential and the current intensity gradually decreases (Fig. 2b). This phenomenon is in agreement with the electrochemical behavior for the majority of the W-waves of POMs. Along with the decreasing pH, the reduction of **1**-CPE is accompanied by the evolution of protons from solution to the surface of the electrode to maintain charge neutrality [34]. Furthermore, the influence of the scan rate on electrochemical behavior of **1**-CPE has also been investigated in the potential range of -1.0 to 1.0 V in the abovementioned conditions (Fig. 2c). As shown in Fig. 2d, the peak current intensities (I_{pc}) are proportional to the scan rates (ν), and its linear equation is $I_{pc} = -0.00000415\nu - 0.00007$ with the correlation coefficient of 0.992, which suggests a surface controlled electron-transfer process occurring at **1**-CPE [35].

The variable temperature magnetic susceptibility for **1** has been preliminarily studied on the polycrystalline sample in the temperature range of 2–300 K at an applied magnetic field of 2000 Oe and the plots of χ_M, $\chi_M T$ and χ_M^{-1} versus T are displayed in Fig. 3. The χ_M value slowly increases from 0.003 emu mol^{-1} at 300 K to 0.023 emu mol^{-1} at 33 K. This rising trend is more pronounced with lowering temperature and exponentially reaches the maximum of 0.21 emu mol^{-1} at 2 K. Correspondingly, at room temperature the $\chi_M T$ for **1** (0.795 emu K mol^{-1}) matches well with that expected for two noninteracting Cu^{II} cations of 0.750 emu K mol^{-1} (with $S = 1/2$, $g = 2.0$). On lowering the
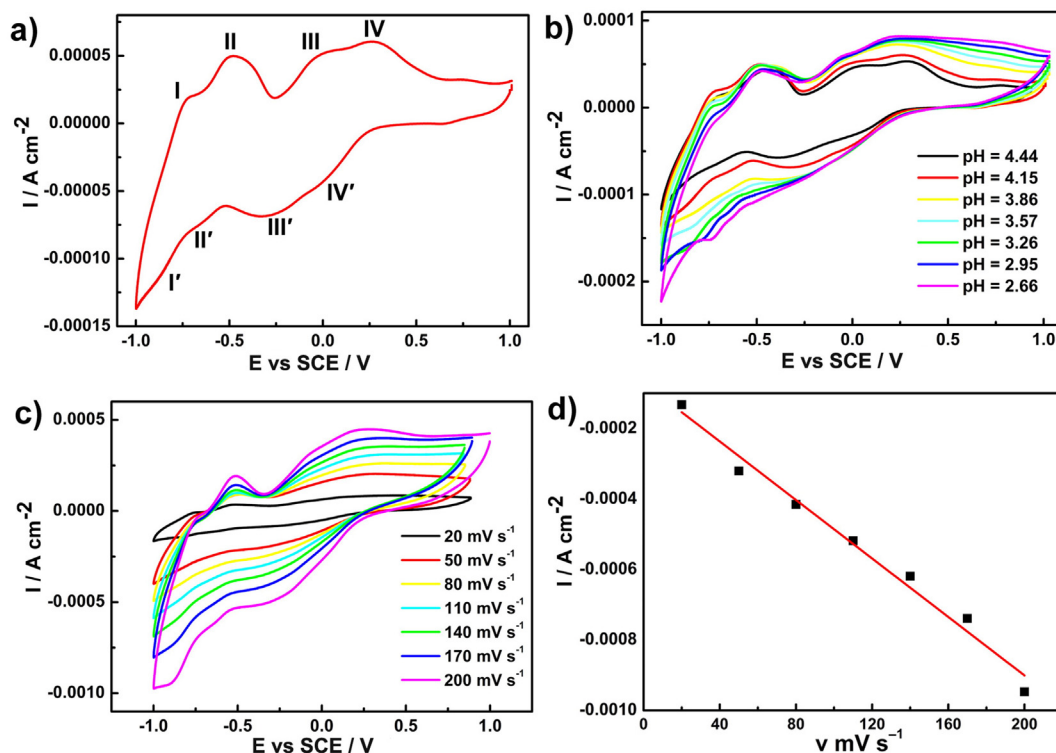

Fig. 2. (a) Cyclic voltammogram of **1**-CPE in pH = 4.15, 0.5 mol·L^{-1} Na$_2$SO$_4$ + H$_2$SO$_4$ aqueous solution. (b) Cyclic voltammograms of **1**-CPE at different pH values. (c) Cyclic voltammograms of **1**-CPE at different scan rates. (d) Variation of cathodic peak currents of the W^{VI}-based wave (I/I′) with the scan rates for **1**-CPE.
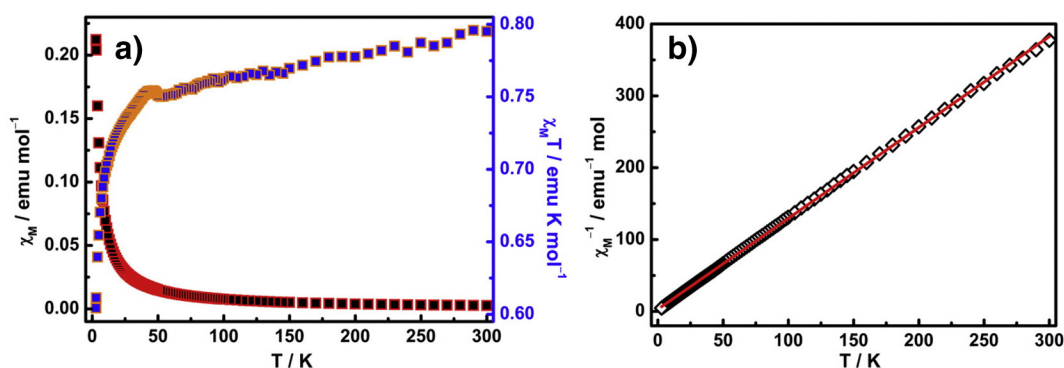
Fig. 3. (a) The temperature dependence of the molar magnetic susceptibility χ_M and the product of the molar magnetic susceptibility and temperature $\chi_M T$ for **1** between 2 and 300 K. (b) Temperature dependence of the reciprocal susceptibility for **1** between 2 and 300 K. The red solid line is generated by the Curies–Weiss expression. (For interpretation of the references to color in this figure legend, the reader is referred to the web version of this article.)

temperature, the $\chi_M T$ gradually drops to 0.604 emu K mol^{-1} at 2 K, indicating the weak antiferromagnetic exchange interactions within Cu^{II} centers mediated by 4,4′-bpy connectors. The magnetic susceptibility data in the range of 300–2 K can be well fitted by the Curie–Weiss expression [$\chi_M = C / (T - \theta)$] with $C = 0.79$ emu K mol^{-1} and $\theta = -2.39$ K. The small negative value of θ confirms the presence of weak antiferromagnetic couplings among the Cu^{II} centers.

In summary, we have hydrothermally obtained an organic–inorganic hybrid independent 1-D double-chain Keggin-type ST **1** with mixed ligands, which was structurally characterized by elemental analyses, IR spectra and single-crystal X-ray diffraction. To the best of our knowledge, **1** represents the first independent organic–inorganic hybrid 1-D double-chain ST in POM chemistry. Its solid-state electrochemical properties have been performed and discussed. Furthermore, the magnetic property of **1** has been studied by the variable-temperature magnetic susceptibility. Currently, we are trying to explore the appropriate reaction conditions so that multi-carboxylic acid ligands and Ln cations can be introduced to the system to manufacture novel PBTLHDs.

Appendix A. Supplementary data

CCDC 1038604 for **1** contains the supplementary crystallographic data for this paper. These data can be obtained free of charge from The Cambridge Crystallographic Data Centre via www.ccdc.cam. ac.uk/data_request/cif. Supplementary data associated with this article can be found in the online version at http://dx.doi.org/10.1016/j.inoche.2015.01.015.

References

[1] P. Gouzerh, A. Proust, Main-group element, organic, and organometallic derivatives of polyoxometalates, Chem. Rev. 98 (1998) 77.

[2] J.-W. Zhao, S.-T. Zheng, G.-Y. Yang, 0-D and 1-D inorganic–organic composite polyoxotungstates constructed from in-situ generated monocopper^{II}-substituted Keggin polyoxoanions and copper^{II}–organoamine complexes, J. Solid State Chem. 181 (2008) 2205.

[3] Y. Kikukawa, Y. Kuroda, K. Yamaguchi, N. Mizuno, Diamond-shaped [Ag$_4$]$^{4+}$ cluster encapsulated by silicotungstate ligands: synthesis and catalysis of hydrolytic oxidation of silanes, Angew. Chem. Int. Ed. 51 (2012) 2434.

[4] L. Yang, X. Ma, P.T. Ma, J.A. Hua, J.Y. Niu, A series of arsenotungstates based on the [HAs$_2$W$_8$O$_{31}$]$^{-7}$ building block: syntheses by control of the reaction process, Cryst. Growth Des. 13 (2013) 2982.

[5] J.W. Zhao, Y.Z. Li, F. Ji, J. Yuan, L.J. Chen, G.Y. Yang, Syntheses, structures and electrochemical properties of a class of 1-D double chain polyoxotungstate hybrids [H$_2$dap][Cu(dap)$_2$]$_{0.5}$[Cu(dap)$_2$(H$_2$O)] [Ln-(H$_2$O)$_3$(α-GeW$_{11}$O$_{39}$)]·3H$_2$O, Dalton Trans. 43 (2014) 5694.

[6] B.S. Bassil, M. Ibrahim, R. Al-Oweini, M. Asano, Z. Wang, J. van Tol, N.S. Dalal, K.Y. Choi, R.N. Biboum, B. Keita, L. Nadjo, U. Kortz, A planar {Mn$_{19}$(OH)$_{12}$}$^{26+}$ unit incorporated in a 60-tungsto-6-silicate polyanion, Angew. Chem. Int. Ed. 50 (2011) 5961.

[7] K. Suzuki, Y. Kikukawa, S. Uchida, H. Tokoro, K. Imoto, S. Ohkoshi, N. Mizuno, Three-dimensional ordered arrays of 58 × 58 × 58 Å^3 hollow frameworks in ionic crystals of M$_2$Zn$_2$-substituted polyoxometalates, Angew. Chem. Int. Ed. 51 (2012) 1597.

[8] L. Yang, Y. Huo, J.Y. Niu, Combination between [B-α-SiW$_9$O$_{34}$] unit and triangular inorganic Ni$_6$ core under hydrothermal conditions: from monomer to rare dimer with malposed dodeca-nickel centers, Dalton Trans. 42 (2013) 364.

[9] G.B. Zhu, Y.V. Geletii, J. Song, C.C. Zhao, E.N. Glass, J. Bacsa, C.L. Hill, Di- and tri-cobalt silicotungstates: synthesis, characterization, and stability studies, Inorg. Chem. 52 (2013) 1018.

[10] L.B. Ni, F. Hussain, B. Spingler, S. Weyeneth, G.R. Patzke, Lanthanoid-containing open Wells–Dawson silicotungstates: synthesis, crystal structures, and properties, Inorg. Chem. 50 (2011) 4944.

[11] S.Z. Li, D.D. Zhang, Y.Y. Guo, P.T. Ma, X.Y. Qiu, J.P. Wang, J.Y. Niu, Keggin polyoxoanion supported organic–inorganic trinuclear lutetium cluster, {Na(H$_2$O)$_3$[Lu(pydc)(H$_2$O)$_3$]$_3$}[SiW$_{12}$O$_{40}$]·26.5H$_2$O, Dalton Trans. 41 (2012) 9885.

[12] K. Suzuki, M. Sugawa, Y. Kikukawa, K. Kamata, K. Yamaguchi, N. Mizuno, Strategic design and refinement of Lewis acid base catalysis by rare-earth-metal-containing polyoxometalates, Inorg. Chem. 51 (2012) 6953.

[13] H.Y. An, Y. Lan, Y.G. Li, E.B. Wang, N. Hao, D.R. Xiao, L.Y. Duan, L. Xu, A novel chain-like polymer constructed from heteropolyanions covalently linked by lanthanide cations: (C$_5$H$_9$NO$_2$)$_7$Cr Mo$_6$H$_6$O$_{24}$)·11H$_2$O (Proline = C$_5$H$_9$NO$_2$), Inorg. Chem. Commun. 7 (2004) 356.

[14] D.Y. Shi, J.W. Zhao, L.J. Chen, P.T. Ma, J.P. Wang, J.Y. Niu, Four types of 1D or 2D organic–inorganic hybrids assembled by arsenotungstates and Cu^{II}–Ln$^{III/IV}$ heterometals, CrystEngComm 14 (2012) 3108.

[15] J.W. Zhao, J. L, L.J. Chen, J. Yuan, H.Y. Li, P.T. Ma, J.P. Wang, J.Y. Niu, Novel 1-D double-chain organic–inorganic hybrid polyoxotungstates constructed from dimeric copper–lanthanide heterometallic silicotungstate units, CrystEngComm 14 (2012) 7981.

[16] J.W. Zhao, J. Luo, L.J. Chen, J. Yuan, H.Y. Li, P.T. Ma, J.P. Wang, J.Y. Niu, Novel 1-D double-chain organic–inorganic hybrid polyoxotungstates constructed from dimeric copper–lanthanide heterometallic silicotungstate units, CrystEngComm 14 (2012) 7981.

[17] J. Luo, C.L. Leng, L.J. Chen, J. Yuan, H.Y. Li, J.W. Zhao, Three 3D organic–inorganic hybrid heterometallic polyoxotungstates assembled from 1:2-type [Ln(α-SiW$_{11}$O$_{39}$)$_2$]$^{13-}$ silicotungstates and [Cu(dap)$_2$]$^{2+}$ linkers, Synth. Met. 162 (2012) 1558.

[18] J. Luo, J.W. Zhao, J. Yuan, Y.Z. Li, L.J. Chen, P.T. Ma, J.P. Wang, J.Y. Niu, An organic–inorganic hybrid 1-D double-chain copper–yttrium heterometallic silicotungstate [Cu(dap)$_2$(H$_2$O)]$_2${Cu(dap)$_2$[α-H$_2$SiW$_{11}$O$_{39}$ Y(H$_2$O)$_2$]$_2$}·10H$_2$O, Inorg. Chem. Commun. 27 (2013) 2713.

[19] Z.M. Zhang, Y.G. Li, S. Yao, E.B. Wang, Y.H. Wang, R. Clérac, Enantiomerically pure chiral Fe$_{28}$ wheels, Angew. Chem. Int. Ed. 48 (2009) 1581.

[20] Crystal data for **1**: C$_{28}$H$_{34}$Cu$_2$N$_{14}$O$_{44}$SiW$_{12}$, $Mr = 3631.96$, monoclinic, space $P2_1/m$, $a = 11.8912(12)$, $b = 16.6705(17)$, $c = 15.5096(16)$ Å, $\alpha = 90$, $\beta = 99.690(2)$, $\gamma = 90$ °, $V = 3030.6(5)$ Å^3, $Z = 2$, $D_c = 3.980$ g · cm^{-3}, $\mu = 2.488$ mm^{-1}, $F(000) = 3223$, $GOOF = 1.010$. Of 15348 total reflections collected, 5472 were unique [$R_{int} = 0.0441$, R_1 (wR_2) = 0.0355 (0.0845)] for 478 parameters and 4768 reflections [$I > 2\sigma(I)$]. Diffraction data were collected on a Bruker Smart APEX II CCD diffractometer with graphite-monochromated Mo Kα radiation ($\lambda = 0.71073$ Å) at 296(2) K. The structure was solved by direct methods and refined by full-matrix least squares on F^2 using the SHELXTL-97 program package. Intensity data were corrected for Lorentz and polarization effects as well as for multi-scan

absorption. No hydrogen atoms associated with water molecules were located from the difference Fourier map. All of the non-hydrogen atoms except for some C, N and O atoms were refined anisotropically. Positions of the hydrogen atoms attached to the carbon and nitrogen atoms were geometrically placed. All hydrogen atoms were refined isotropically as a riding mode using the default SHELXTL parameters.

[21] B. Li, J.W. Zhao, S.T. Zheng, G.Y. Yang, Inorg. Chem. 48 (2009) 8294.

[22] M. Sadakane, M.H. Dickman, M.T. Pope, Controlled assembly of polyoxometalates chains from lacunary building blocks and lanthanide-cation linkers, Angew. Chem. Int. Ed. 39 (2000) 2914.

[23] P. Mialane, L. Lisnard, A. Mallard, J. Marrot, E. Antic-Fidancev, P. Aschehoug, D. Vivien, F. Sécheresse, Solid-state and solution studies of $\{Ln_n(SiW_{11}O_{39})\}$ polyoxoanions: an example of building block condensation dependent on the nature of the rare earth, Inorg. Chem. 2 (2003) 2102.

[24] J.Y. Niu, J.W. Zhao, J.P. Wang, Synthesis, crystal structure and characterization of a praseodymium[III]-substituted silicotungstate with a novel 1D chain connection motif, Inorg. Chem. Commun. 7 (2004) 876.

[25] J.P. Wang, J.W. Zhao, X.Y. Duan, J.Y. Niu, Syntheses and structures of one- and two-dimensional organic-inorganic hybrid rare earth derivatives based on monovacant Keggin-type polyoxotungstates, Cryst. Growth Des. 6 (2006) 507.

[26] J.D. Compain, P. Mialane, A. Dolbecq, I.M. Mbomekallé, J. Marrot, F. Sécheresse, C. Duboc, E. Rivière, Structural, magnetic, EPR, and electrochemical characterizations of a spin-frustrated trinuclear Cr[III] polyoxometalate and study of its reactivity with lanthanum cations, Inorg. Chem. 49 (2010) 2851.

[27] S.Q. Liu, Z.Y. Tang, Z.X. Wang, Z.Q. Peng, E.K. Wang, S.J. Dong, Oriented polyoxometalate–polycation multilayers on a carbon substrate, J. Mater. Chem. 10 (2000) 2727.

[28] L. Lisnard, A. Dolbecq, P. Mialane, J. Marrot, E. Codjovi, F. Sécheresse, Molecular and multidimensional polyoxotungstates functionalized by $\{Cu(bpy)\}^{2+}$ groups, Dalton Trans. (2005) 3913.

[29] M.-L. Wei, J.-H. Wang, Y.-X. Wang, Two proton-conductive hybrids based on 2,2'-biimidazole molecules and Keggin-type heteropolyacids, J. Solid State Chem. 198 (2013) 323.

[30] J. Toth, F. Anson, Electrocatalytic reduction of nitrite and nitric oxide to ammonia with iron-substituted polyoxotungstates, J. Am. Chem. Soc. 111 (1989) 2444.

[31] P.P. Zhang, J. Peng, X.Q. Shen, Z.G. Han, A.X. Tian, H.J. Pang, J.Q. Sha, Y. Chen, M. Zhu, A twofold interpenetrating framework based on the α-metatungstates, J. Solid State Chem. 182 (2009) 3399.

[32] B. Keita, L.J. Nadjo, New aspects of the electrochemistry of heteropolyacids: part IV. Acidity dependent cyclic voltammetric behaviour of phosphotungstic and silicotungstic heteropolyanions in water and N, N-dimethylformamide, J. Electroanal. 227 (1987) 77.

[33] Z.F. Zhao, B.B. Zhou, Z.H. Su, H.Y. Ma, Hydrothermal synthesis, structure and properties of copper–bipyridine complexes substituted monovacant Keggin arsenotungstate, Solid State Sci. 12 (2010) 803.

[34] J.W. Zhao, D.Y. Shi, L.J. Chen, P.T. Ma, J.P. Wang, J. Zhang, J.Y. Niu, Tetrahedral polyoxometalate nanoclusters with tetrameric rare-earth cores and germanotungstate vertexes, Cryst. Growth Des. 13 (2013) 4368.

[35] M. Sadakane, E. Streckhan, Electrochemical properties of polyoxometalates as electrocatalysts, Chem. Rev. 98 (1998) 219.